Frequency band-gap measurement of two-dimensional air/silicon phononic crystals using layered slanted finger interdigital transducers

Tsung-Tsong Wu,[a] Liang-Chen Wu, and Zi-Gui Huang[b]
Institute of Applied Mechanics, National Taiwan University, Taipei 106, Taiwan

(Received 6 October 2004; accepted 22 February 2005; published online 27 April 2005)

In this paper, we investigate the frequency band-gap features of micromachined air/silicon phononic band structures using layered slanted finger interdigital transducers (SFIT). In order to achieve the applications of phononic crystals on the microelectromechanical system related components, the frequency band-gap widths of surface waves are studied both theoretically and experimentally in micrometer scale phononic crystals. For further integration with the complementary metal-oxide semiconductor processing techniques, silicon is chosen as the base material of the two-dimensional phononic crystals in this study. To cover the frequency band-gap width of the phononic crystal, the wideband SFIT- and the SFIT/ZnO/Si-layered structures in the measurement are analyzed and discussed. For layered structures, the dispersive relation is calculated by the effective permittivity approach, and the frequency response of the layered SFIT is then simulated by the coupling-of-modes model. The frequency band-gap width and the frequency range of two-dimensional air/silicon phononic crystals in micrometer scale are measured, and the result agrees well with the theoretical evaluation. © *2005 American Institute of Physics*.
[DOI: 10.1063/1.1893209]

I. INTRODUCTION

The so-called photonic crystals are periodic dielectric composite structures. Owing to the periodicity, incident waves would interfere with the reflective waves as the electromagnetic (EM) waves propagate through the crystals.[1,2] As a result, the frequency band-gap features occur to prohibit the EM waves of specific frequencies from traveling through the band structures. By the analogy between photon and phonon, repetitive composite structures that are made up of different elastic materials can also prevent elastic waves of some certain frequencies from passing by, i.e., the frequency band-gap features also exist in acoustic waves.[3] Theoretical calculations of bulk acoustic waves in phononic band structures of two-dimensional periodic composites were reported using the plane-wave expansion (PWE) method.[4,5] Except for the PWE method, the layered multiple-scattering theory was applied to study the frequency band gaps of bulk acoustic waves in three-dimensional periodic acoustic composites and the band structure of a phononic crystal consisting of complex and frequency-dependent Lame coefficients.[6,7] In addition, the finite-difference time-domain (FDTD) method was applied to predict exactly the transmission properties of slabs of phononic crystals and to interpret the experimental data of two-dimensional systems.[8–10]

The frequency band-gap features of surface modes are studied mainly using PWE and variational methods.[11–23] Tanaka and Tamura[11,12] and Tanaka *et al.*[13] proposed the theory of surface waves propagating in two-dimensional phononic crystals consisting of two cubic materials in square lattice, and also explained the stop band distribution of the surface, pseudosurface, and bulk waves using the PWE method. Recently, Wu *et al.*[14] and Wu and Huang[15] extended the theory to describe the phononic crystals consisting of materials with general anisotropy, and discussed the level repulsion of bulk acoustic waves in periodic composite materials. Huang and Wu[16] also investigated the temperature effect on frequency band gaps of surface and bulk acoustic waves in phononic crystals.

There are literatures aimed at experimentally studying the surface acoustic waves (SAW) in phononic band structures.[17–23] The detection and control of the high-frequency (bulk acoustic waves) sound have been investigated in a dual-core square-lattice photonic crystal fiber perform using the interferometric setup.[17] Vines *et al.*[18] and Vines and Wolfe[19] conducted an experimental study on the surface waves generated by a line-focus acoustic lens at the water-loaded surfaces of a number of two-dimensional superlattices that intersect the surface normally. The propagation of Scholte-like acoustic waves at the liquid-loaded surfaces of periodic structures has also been studied.[20] Rayleigh-wave attenuation in a semi-infinite two-dimensional elastic-band-gap crystal, and surface-state phenomena in linear and point defects were reported and discussed.[21,22] Recently, Wu *et al.*[23] investigated the frequency band-gap features of surface waves in micromachined air/silicon phononic structures in both theoretical and experimental ways.

The concept of employing the slanted finger interdigital transducer (SFIT) as wideband filters was first proposed by Hyodo *et al.*[24] Campbell *et al.*[25] and Campbell[26] have done numerous experiments and designs for SFIT SAW filters and brought up three methods to modify the pass-band inclination phenomenon of SFIT. Yatsuda *et al.*[27] and Yatsuda[28,29] applied the single-phase unidirectional transducer (SPUDT),

[a]Electronic mail: wutt@ndt.iam.ntu.edu.tw
[b]Electronic mail: huang@ndt.iam.ntu.edu.tw

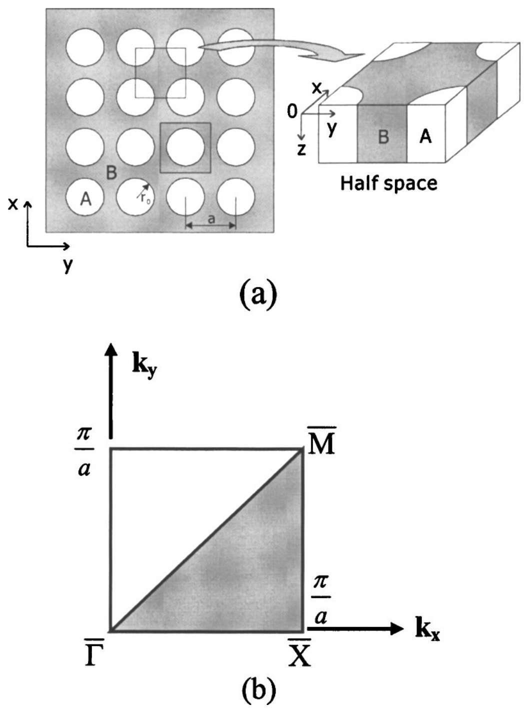

FIG. 1. (a) Two-dimensional phononic crystals with a square lattice; (b) surface Brillouin zone of a square lattice.

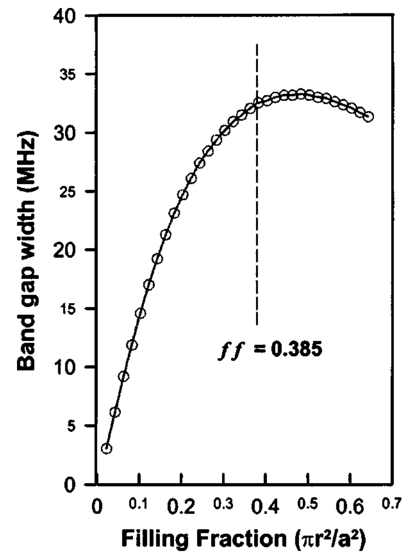

FIG. 2. The relation between the frequency band-gap width and the filling fraction.

withdrawal weighted and aperture weighted, on the design of SFIT to meet the wideband filter requirements for low-insertion loss and low-shape factor.

The purpose of this study is to measure the frequency band gap of SAW modes in two-dimensional air/silicon phononic crystals with micrometer scale using wideband SFIT. In the following, analysis of frequency band gaps in two-dimensional air/silicon phononic crystals is given and discussed. The simulated response of a layered SFIT SAW filter is followed. Then we describe the fabrication and measurement of a two-dimensional phononic crystal, with dimensions in the order of micrometer.

II. THEORETICAL SIMULATION AND EXPERIMENTAL DESIGN

In this study, we adopt the PWE method to calculate the frequency band gaps of surface acoustic waves in two-dimensional phononic crystals.[14] In order to fabricate the phononic crystal in micrometer scale and to further integrate with the CMOS process, silicon is chosen as the substrate material. The simplest structure of a silicon-based phononic crystal is the one with vacuum or air-filled cylindrical holes. Besides, for the potential to develop the phononic crystals as a device, the SAW modes are selected to propagate in the band structures.

A two-dimensional phononic crystal with a square lattice consisting of a circular cylinder (A) embedded in a background material (B) with lattice spacing a is considered and shown in Fig. 1(a). Figure 1(b) is the surface Brillouin region of a square lattice in which the reciprocal lattice vector is $\mathbf{G}=(2\pi N_1/a, 2\pi N_2/a)$, where N_1, $N_2=0,\pm1,\pm2,\ldots$ and the filling fraction is $ff=\pi r_0^2/a^2$. The irreducible part of the surface Brillouin zone of a square lattice is shown in Fig. 1(b), which is a triangle with vertices $\overline{\Gamma}$, $\overline{X}$, and $\overline{M}$.

Considering the air/silicon phononic crystal with a square lattice, the filling fraction ff is 0.385, i.e., $r_0/a=0.35$. In this paper, we consider a phononic crystal consisting of a silicon substrate and square arrays of air cylindrical holes. The modified PWE method can be well approximately used because of the high-density contrast between solid and air. It is well-known that the high-density contrast between solid and air leads to the unexpected flat bands in the band structure. We get rid of this problem by adopting the technique reported in Refs. 23 and 30, in which an artificial transverse velocity of the fluid has been used. In the case of a vacuum/solid band structure, the density and elastic constants of the holes can be set as zero to satisfy the traction-free condition.[31]

In Fig. 2, the surface wave frequencies ω_1 and ω_2, and the width of the frequency band gap $\Delta\omega=\omega_2-\omega_1$ at the $\overline{X}$ point are plotted as functions of the filling fraction ff.[23] The maximum frequency band-gap width occurs at about $ff=0.48$. For the potential application on realizing the microacoustic channel, the frequency band-gap width and the angular magnitude that surface waves can propagate have to be taken into account at the same time. Moreover, for the sake of convenience, the value $ff=0.385$ is selected to draw the photo mask in this paper.

The objective of this study is to measure the frequency band gap of surface waves in two-dimensional air/silicon phononic crystals. Therefore, a high-frequency wideband SAW transducer on the silicon substrate is used to generate and detect the signals. Besides, because silicon is not a piezoelectric material, the layered structure SFIT/ZnO/silicon has to be considered in the device. As to the corresponding design parameters, it will depend upon the band-gap frequency of the two-dimensional phononic crystals.

The evaluation of band-gap frequencies along the x axis in two-dimensional air/silicon phononic crystals are from 183 to 215 MHz. Considering the fabrication difficulty in

TABLE I. Design parameters of the SFIT/ZnO/silicon-layered structure.

	ZnO(2 μm)/Si			
Substrate Design No.	1	2	3	4
Center frequency (MHz)	200	195	215	185
Bandwidth (%)	~35	~24	~28	~28
λ_{min}(μm)	17	18	16	19
λ_{max}(μm)	25	24	22	26
Input pairs (pairs)	40	40	40	40
Output pairs (pairs)	32	32	32	32
Metal thickness (Å)	1600	1600	1600	1600
Propagation length (μm)	631.25	606	489.5	656.5
Aperture (μm)	2500	2400	2200	2600
Max. tilt angle (degree)	3.66	2.86	3.12	3.08

this experiment, the lattice constant is chosen as 10 μm, and the radius of the circular cylinder r_0 is thus equal to 3.5 μm. According to the band-gap frequencies, the corresponding design parameters are listed in Table I. In design 1, the band-gap frequencies are located at the center of the pass band of the layered SFIT. Therefore, the frequency band-gap width of phononic crystals can be measured by this experimental setup. Figure 3 is the schematic diagram of this experiment. The SFIT are on the top of the layered structure. There are six rows of cylinders filled with air between the interdigital transducer (IDT) pairs. The filtering efficiency can be roughly understood by this arrangement.

III. ANALYSIS OF LAYERED SFIT SAW FILTER

Unlike the half-space SAW filter, the phase velocity of a layered SAW is dispersive. Consequently, the dispersion has to be considered in the design of a layered SAW filter. The SAW dispersion relation of the layered system has been studied using the effective permittivity method.[32]

Figure 4(a) shows the phase velocity dispersion of the zeroth and first SAW modes in (0001)ZnO/(001)[100]Si layered structure with free-surface boundary condition. The horizontal axis represents the product of the frequency and the thickness of ZnO thin film, while the vertical axis is the phase velocity of the SAW. The results show that the phase velocity decreases as the frequency thickness fh_{ZnO} increases because the phase velocity of ZnO is slower than that of silicon. For a layered SAW device, the electromechanical coupling coefficient varies with different boundary

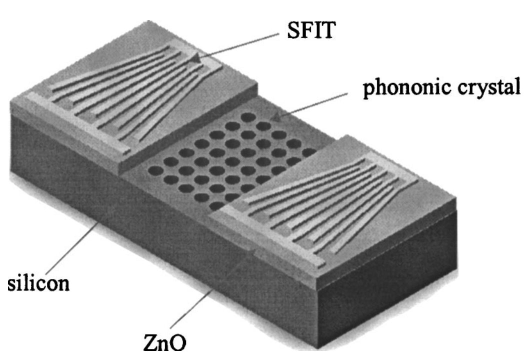

FIG. 3. The schematic diagram of this experimental setup.

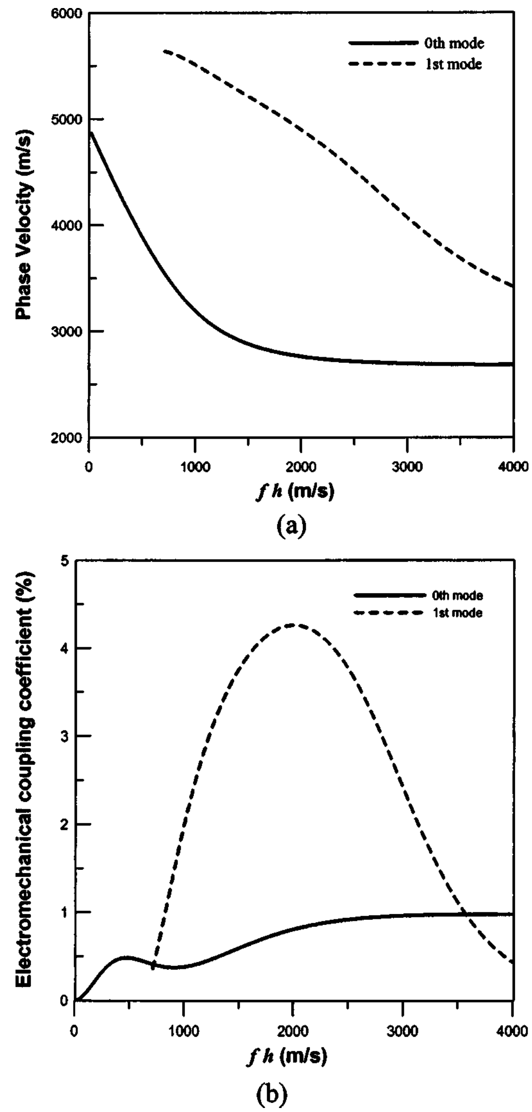

FIG. 4. ZnO/Si SAW dispersion relation. (a) phase velocity dispersion curve; (b) electromechanical coupling coefficient dispersion curve.

conditions.[33–35] Hence, by varying the boundary conditions, the proper layered structure will have a strong piezoelectric property. Figure 4(b) is the electromechanical coupling coefficient dispersion of the IDT/ZnO/silicon-layered structure. The horizontal axis represents the product of the frequency and the thickness of ZnO thin film, and the vertical axis is the corresponding electromechanical coupling coefficient k^2. The solid line denotes the zeroth mode and the dashed line is the first mode. From this figure, the first mode has a higher electromechanical coupling coefficient than the zeroth mode, which means the first mode is more appropriate for the design of a layered SFIT. However, the zeroth mode is chosen to design the layered SFIT in this study, considering the limitation of our current fabrication facilities.

The main difference between a layered and a half-space structure is that the phase velocity and electromechanical coupling coefficient are dispersive, not a constant. So when we employ the coupling-of-modes (COM) model[36] to analyze a layered SAW filter, some of the COM parameters become frequency-dependent and have to be considered in the analysis.[37] The dispersive COM parameters in layered struc-

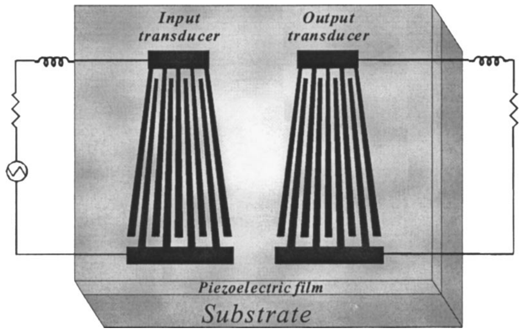

FIG. 5. Layered SFIT SAW filter.

tures include the phase velocity shift, reflection coefficient, transduction coefficient, IDT capacitance, and propagation loss. As far as the dispersion is concerned, the formulas of these COM parameters can be adopted to analyze the layered SAW devices.

It is worth noting that the propagation loss γ of commonly used half-space substrates such as quartz and $LiNbO_3$ can be obtained from an approximated formula,[38] while there is no formula that can be used for layered structures. Thus the propagation loss γ of a layered structure has to be measured experimentally. Moreover, because the frequency range of this study is not small as in the case of a layered SFIT, we *cannot* assume that the variation of propagation loss is independent of the frequency. Therefore, in this study, the frequency-dependent propagation loss obtained from the experiment should be substituted into the COM model to compare with the simulations.

Based on the modified COM parameters including the SAW dispersion effect, the frequency response of layered SFIT (Fig. 5) can then be calculated.[39] The general approach used to analyze the slanted finger interdigital transducer is to divide the electrode of SFIT SAW filter into *n* sections by the equal aperture separation or equal center-frequency separation method.[27] In this study, the SFIT/ZnO/Si-layered wideband SAW filters are considered according to the fabrication process of two-dimensional microscale phononic crystals. The thickness of ZnO thin film is chosen as 2 μm, and the design parameters are listed in Table I. The corresponding parameters are demonstrated in Fig. 6. The simulated frequency responses (design 1) of the layered SFIT, regarding and disregarding the dispersion effect, are shown in Fig. 7.

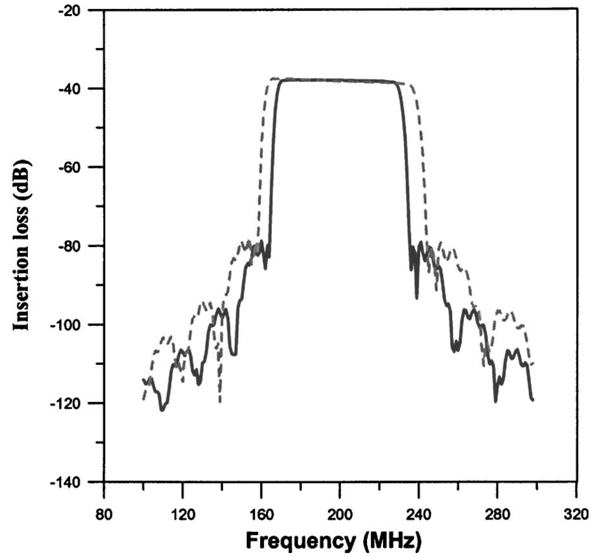

FIG. 7. Dispersive and nondispersive frequency responses.

The center frequency is about 200 MHz. The results show that the frequency bandwidth calculated with the dispersion effect is narrower than that obtained without the dispersion. As shown in Fig. 4(a), the phase velocity of the fundamental mode in the SFIT/ZnO/Si-layered structure decreases as the frequency increases. Therefore, when the dispersion effect is considered, the bandwidth of the SFIT/ZnO/Si-layered wideband SAW filters will reduce quite obviously.

IV. EXPERIMENTAL RESULTS

The frequency response of SFIT/ZnO/Si can be obtained by the modified COM model. In general, some of the COM parameters used in the simulation are not consistent with the experimental results. Therefore, the measured COM parameters should be resubstituted into the COM model to acquire exact simulated frequency responses. Here we utilize the time-gating approach to neglect the electromagnetic feedthrough effect[40] and the triple transit echo. Figure 8 shows the microscopic pictures of the layered SFIT.

A. Modification of frequency responses

Because the actual parameters of the layered SFIT somewhat differs from the expected designed parameters, the

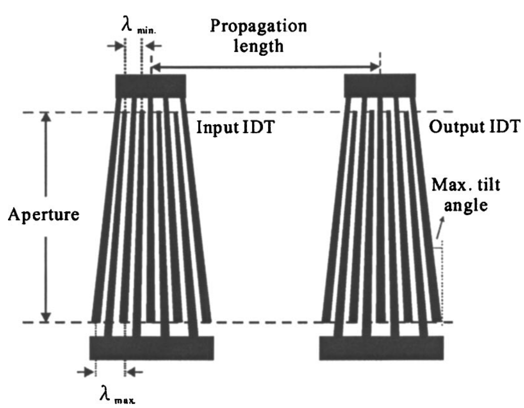

FIG. 6. Illustration of design parameters.

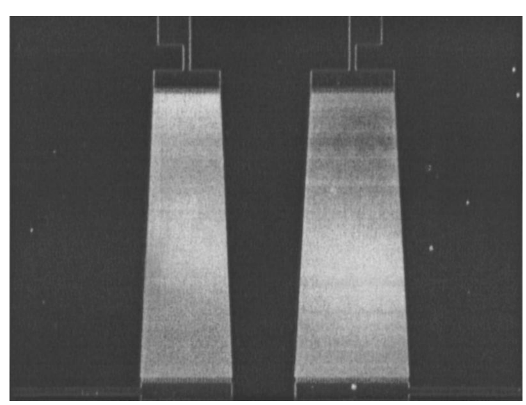

FIG. 8. A microscopic picture of the fabricated layered SFIT.

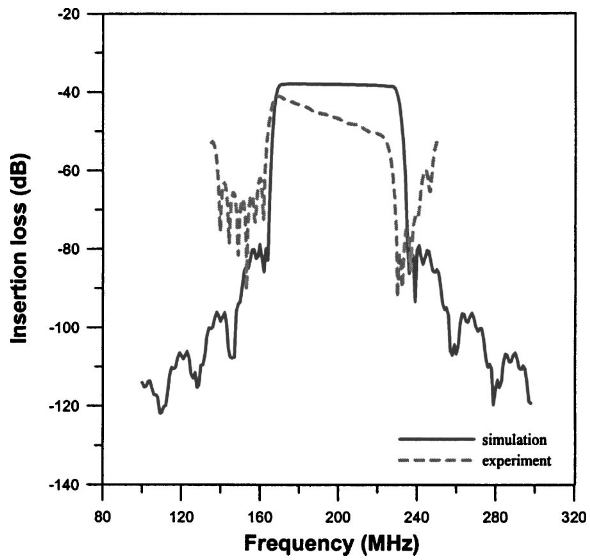

FIG. 9. The comparison of unmodified simulation responses and experimental results of design 1.

simulation of frequency response has to be modified. Figure 9 shows the comparison between the unmodified simulation responses under the assumption of no propagation losses and the experimental results (design 1). It can be observed that the pass band is slightly shifted and inclined downward. Also, the insertion loss is higher than that of the simulation because the propagation loss does not vanish. Therefore, the actual parameters have to be measured in order to obtain correct responses.

The phase velocity dispersion of layered structures will be changed when the thickness of the ZnO thin film is not as expected. In addition, the thickness of the metal electrodes also affects the phase velocity due to the mass loading effects. Therefore, the actual thickness of the ZnO thin film and the actual thickness of the metal electrodes have to be substituted into the COM model to obtain the modified simulations. The deposited ZnO thin-film thickness is 2.20 μm and the measured thickness of the SFIT electrodes is 2742 Å. The comparison between the simulated response with modified phase velocity and the experimental result of design 1 is shown in Fig. 10(a). The result shows that the bandwidth and the pass-band frequency in this experiment have matched the simulated frequency response.

After the modification of the phase velocity in layered structures, it can be found that there exists a difference of insertion loss between the experimental results and the simulated responses. It is due to the assumption of zero propagation loss in the simulations. To cover the overall loss of the SFIT SAW device, a linear relation between the propagation loss and the frequency has been calculated inversely, based on the experimental result of design 1. Figure 10(b) shows the dispersive relation of the propagation loss. The propagation loss at the center frequency of 200 MHz is 50 dB/cm, which is a reasonable value compared with the experimental results[35] of Nakahata *et al.*, $\gamma = 50$ dB/cm. From these results, the pass bands of the layered SFIT are all inclined downward at the high-frequency part due to the propagation losses. The propagation loss we define here includes the attenuation of surface wave propagation, the ohmic loss due to the shape of the SFIT electrode, and the diffraction effect.

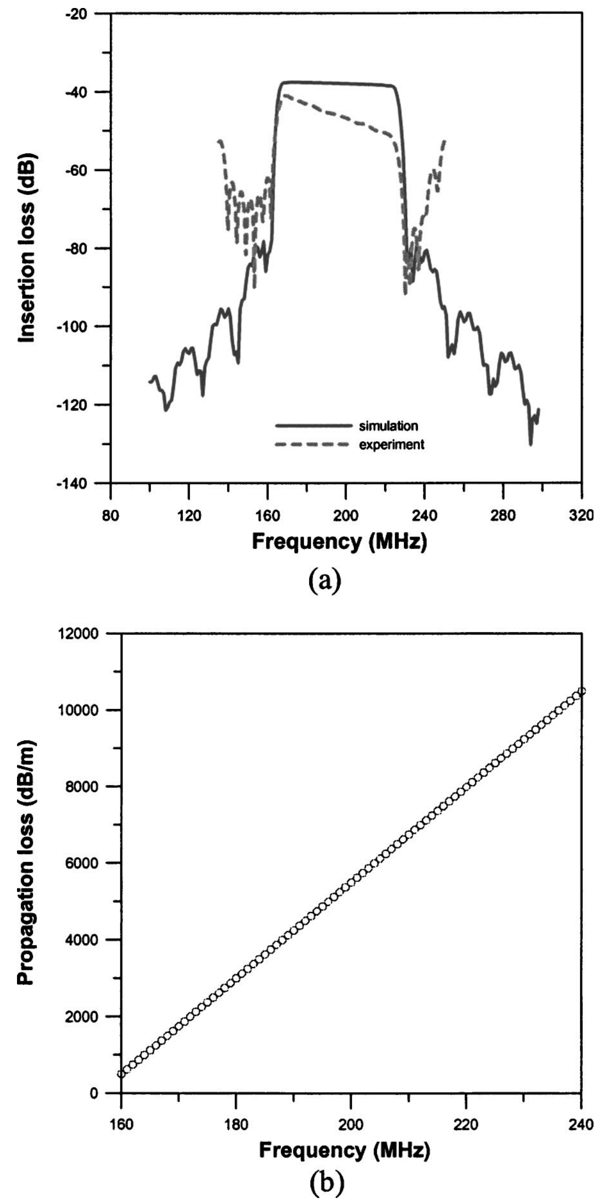

FIG. 10. (a) Comparison of frequency responses with modified phase velocity (design 1); (b) the dispersive relation of propagation loss.

B. Measurement of frequency band gap

Two-dimensional silicon-based phononic crystals consisting of six rows of air cylinders are fabricated and shown in Fig. 11(a). On both sides of the figures are the SFIT on the ZnO thin films. Figure 11(b) is the cross section of the two-dimensional air/silicon phononic crystals. The physical characteristics of this experimental setup are mentioned in Sec. II, i.e., the lattice constant $a = 10$ μm, the radius of the circular cylinder $r_0 = 3.5$ μm, and the filling fraction $ff = 0.385$. The predicted frequency band gap along the x axis is located between 183 and 215 MHz. Figure 11(b) shows a finite slab of a phononic crystal, while the depths of the two-dimensional periodic cylinders are fabricated at least 80 μm. Because the energy of SAW modes is mostly confined to a

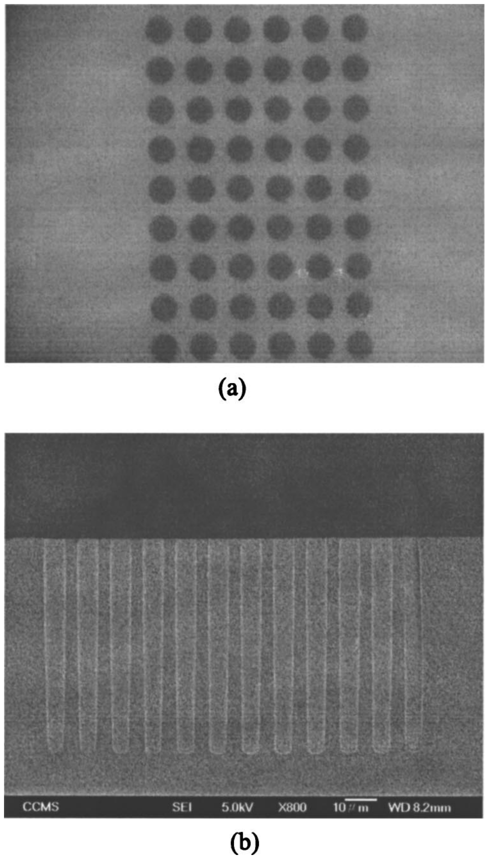

FIG. 11. (a) A microscopic picture of two-dimensional phononic crystals; (b) cross section of two-dimensional phononic crystals.

depth of one to two wavelengths of the SAW, the finite slab is suitable for discussing the frequency band-gap features of SAW modes.

In Fig. 12, the frequency band gaps of the air/silicon phononic crystals are revealed by the layered SFIT of design 1 in the range of pass-band frequency. The shadow region

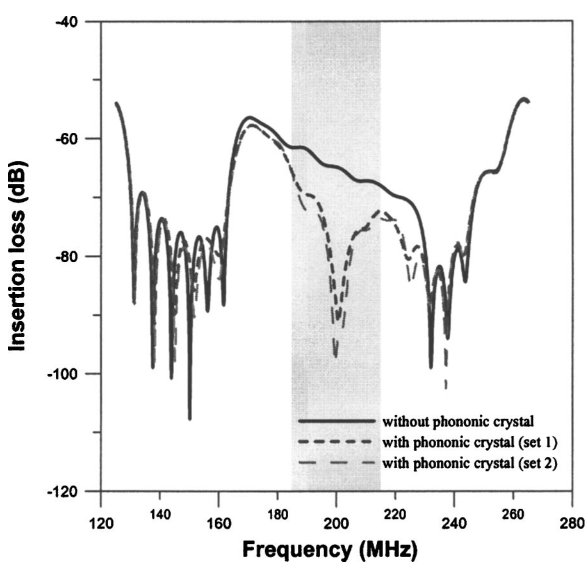

FIG. 12. The frequency band gaps of the phononic crystals are revealed by the layered SFIT of design 1 in the range of pass-band frequency. The shadow region represents the frequency band gap of fabricated phononic crystals with six rows of air cylinders.

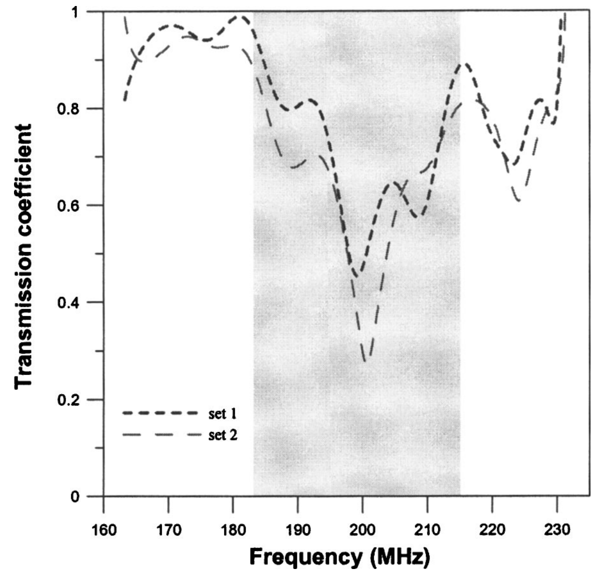

FIG. 13. The acoustic transmission coefficient.

represents the frequency band gap of fabricated phononic crystals with six rows of air cylinders. The dashed line and solid lines denote the measurements with and without phononic crystals, respectively. The two dashed lines are the results of different sets with the same design. We can find that the insertion loss that is measured with phononic crystals in the range of pass-band frequency is clearly lower than the results without phononic crystals. Most of the SAW energy is blocked by phononic band structures. The result shows good agreement with the theoretical evaluation by the PWE method.

Furthermore, if we divide the insertion loss of the SFIT system with phononic band structures by that without phononic band structures, the transmission coefficients can then be obtained (Fig. 13). The acoustic transmission coefficient clearly shows that the surface waves are attenuated greatly in the forbidden band. Moreover, because the propagation loss increases with the decrease of wavelength, the transmission coefficient at the upper edge of the stop band is not as high as expected, i.e., equals 1. On the other hand, the experimental results from the parameters in designs 2, 3, and 4 (Table I) also validate the similar results in this paper.

V. CONCLUSION

In this paper, we introduced the layered SFIT to measure the band-gap width of a two-dimensional phononic crystal. The COM model was utilized to simulate the frequency response of the layered SFIT and the simulation showed good agreement with the measured response. In the band-gap study, the frequency band-gap width and frequency range of the two-dimensional air/silicon phononic crystals with dimensions in micrometer scales are successfully measured by the layered SFIT, and showed clearly the predicted frequency band-gap width. This experimental verification can further be exploited for the applications of phononic crystals on MEMS-related components, such as filters, guiding acoustic waves, or microacoustic channels.

ACKNOWLEDGMENTS

The authors thank the National Science Council (NSC93-2212-E-002-025) and the NTU-ITRI Center of Taiwan for the financial support.

[1] S. G. Johnson, and J. D. Joannopoulos, *Photonic Crystals: The Road From Theory To Practice* (Kluwer, Boston, 2003).
[2] J. D. Joannopoulos, R. D. Meade, and J. N. Winn, *Photonic Crystals: Molding The Flow Of Light* (Princeton University Press, Princeton, NJ, 1995).
[3] A. Modinos, N. Stefanou, I. E. Psarobas, and V. Yannopapas, Physica B **296**, 167 (2001).
[4] M. Sigalas and E. N. Ecconomou, J. Sound Vib. **158**, 377 (1992).
[5] M. S. Kushwaha, P. Halevi, L. Dobrzynski, and B. Djafari-Rouhani, Phys. Rev. Lett. **71**, 2022 (1993).
[6] I. E. Psarobas, N. Stefanou, and A. Modinos, Phys. Rev. B **62**, 278 (2000).
[7] Z. Liu, C. T. Chen, P. Sheng, A. L. Goetzen, and J. H. Page, Phys. Rev. B **62**, 2446 (2000).
[8] D. Garcia-Pablos, M. Sigalas, F. R. Montero de Espinoza, M. Torres, M. Kafesaki, and N. Garcia, Phys. Rev. Lett. **84**, 4349 (2000).
[9] M. Sigalas and N. Garcia, J. Appl. Phys. **87**, 3122 (2000).
[10] M. Sigalas and N. Garcia, Appl. Phys. Lett. **76**, 2307 (2000).
[11] Y. Tanaka and S. Tamura, Phys. Rev. B **58**, 7958 (1998).
[12] Y. Tanaka and S. Tamura, Phys. Rev. B **60**, 13294 (1999).
[13] Y. Tanaka, Y. Tomoyasu, and S. Tamura, Phys. Rev. B **62**, 7387 (2000).
[14] T.-T. Wu, Z. G. Huang, and S. Lin, Phys. Rev. B **69**, 094301 (2004).
[15] T.-T. Wu and Z. G. Huang, Phys. Rev. B **70**, 214304 (2004).
[16] Z. G. Huang and T.-T. Wu, IEEE Trans. Ultrason. Ferroelectr. Freq. Control **52**, 365 (2005).
[17] P. St. J. Russell, E. Marin, and A. Díez, Opt. Express **11**, 2555 (2003).
[18] R. E. Vines, J. P. Wolfe, and A. G. Every, Phys. Rev. B **60**, 11871 (1999).
[19] R. E. Vines and J. P. Wolfe, Physica B **263-264**, 567 (1999).
[20] A. G. Every, R. E. Vines, and J. P. Wolfe, Phys. Rev. B **60**, 11755 (1999).
[21] F. Meseguer, M. Holgado, D. Caballero, N. Benaches, J. Sa'nchez-Dehesa, C. Lo'pez, and J. Llinares, Phys. Rev. B **59**, 12169 (1999).
[22] M. Torres, F. R. Montero de Espinosa, D. Garica-Pablos, and N. Garcia, Phys. Rev. Lett. **82**, 3054 (1999).
[23] T.-T. Wu, Z. G. Huang, and S. Y. Liu, Zeitschrift für Kristallographie (in press).
[24] T. Hyodo, K. Yamanouchi, and K. Shibayama, *Proc. Acoustic Society of Japan 1968 Autumn Annual Meeting*, 3-1-14, 193 (in Japanese) (1968).
[25] C. K. Campbell, Y. Ye, and J. J. Sferrazza PaPa, IEEE Trans. Sonics Ultrason., **SU-29**, 224 (1982).
[26] C. K. Campbell, *Surface Acoustic Wave Devices for Mobile and Wireless Communications* (Academic, San Diego, 1998).
[27] H. Yatsuda, Y. Takeuchi, and S. Yoshikawa, Proc.-IEEE Ultrason. Symp. 61 (1990).
[28] H. Yatsuda, IEEE Trans. Ultrason. Ferroelectr. Freq. Control **44**, 453 (1997).
[29] H. Yatsuda, IEEE Trans. Ultrason. Ferroelectr. Freq. Control **45**, 41 (1998).
[30] C. Goffaux and J. P. Vigneron, Phys. Rev. B **64**, 075118 (2001).
[31] V. Laude, M. Wilm, S. Benchabane, and A. Khelif, Phys. Rev. E **71**, 036607 (2005).
[32] T.-T. Wu and Y. Y. Chen, IEEE Trans. Ultrason. Ferroelectr. Freq. Control **49**, 142 (2002).
[33] K. Tsubouchi, K. Sugai, and N. Mikoshiba, Proc.-IEEE Ultrason. Symp. 375 (1981).
[34] H. Nakahata, A. Hachigo, K. Higaki, S. Fujii, and S. Shikata, IEEE Trans. Ultrason. Ferroelectr. Freq. Control **42**, 362 (1995).
[35] H. Nakahata, K. Higaki, S. Fujii, A. Hachigo, H. Kitabayashi, K. Tanabe, Y. Seki, and S. Shikata, Proc.-IEEE Ultrason. Symp. 361 (1995).
[36] B. P. Abbott, Proc.-IEEE Ultrason. Symp. 5 (1991).
[37] Y. Y. Chen, T.-T. Wu, and T. T. Chou, J. Phys. D **37**, 120 (2004).
[38] D. P. Morgan, *Surface-Wave Devices for Signal Processing* (Elsevier, New York, 1985).
[39] T.-T. Wu and C. M. Lin, J. Chin. Inst. Eng. **27**, 973 (2004).
[40] J. H. Visser and A. Venema, Proc.-IEEE Ultrason. Symp. 297 (1988).